Diplomarbeit

RNA EXPRESSION ANALYSIS OF SELECTED COMPONENTS OF SPHINGOLIPID METABOLISM IN PRIMARY PORCINE MICROVASCULAR BRAIN ENDOTHELIAL CELLS

eingereicht von

Kwasi Takyi Osei-Tutu

zur Erlangung des akademischen Grades

Doktor der gesamten Heilkunde

(Dr. med. univ.)

an der

Medizinischen Universität Graz

ausgeführt am

Lehrstuhl für Molekularbiologie und Biochemie

unter der Anleitung von

Ao. Univ.-Prof. Dr.rer.nat Wolfgang Sattler

Sen. Lecturer Dr.rer.nat Eva Bernhart

Graz, am 05.02.2021

Eidesstattliche Erklärung

Ich erkläre ehrenwörtlich, dass ich die vorliegende Arbeit selbstständig und ohne fremde Hilfe verfasst habe, andere als die angegebenen Quellen nicht verwendet habe und die den benutzten Quellen wörtlich oder inhaltlich entnommenen Stellen als solche kenntlich gemacht habe.

Graz, am 05.02.2021 *Kwasi Takyi Osei-Tutu eh.*

Acknowledgments

I owe it all to Almighty God, who has brought me this far. Blessed be the name of the Lord.

First, I would like to express my sincere gratitude to my supervisors, Ao. Univ.-Prof. Dr.rer.nat Wolfgang Sattler and Sen. Lecturer Dr.rer.nat Eva Bernhart. It has been a true honor being your thesis student.

I would like to thank Professor Sattler's team as well as the entire staff of the Institute of molecular biology and chemistry for sharing their knowledge in lab skills and science with me. I am especially grateful to Dr Andrea Wintersperger for her kind and competent support. I sincerely appreciate the pleasant atmosphere.

Many thanks to my family for their kind support in all endeavors.

Saving the best for last – dear Erika, I am very grateful.

May the Lord richly bless you all.

Graz, 05.02.2021

Table of Contents

Abbreviations

2-ClHDA	2-chlorohexadecanal
ACER1	alkaline ceramidase 1
ACER2	alkaline ceramidase 2
ACER3	alkaline ceramidase 3
AD	Alzheimer’s disease
AJ	adherens junction
ASAH1	N-Acylsphingosine amidohydrolase 1
ASAH2	N-Acylsphingosine amidohydrolase 2
ATX	autotaxin
BBB	blood-brain barrier
BCEC	brain capillary endothelial cells
bFGF	basic fibroblast growth factor
BMVEC	brain microvascular endothelial cell
cDNA	complementary DNA
CerS1	ceramide synthase 1
CERS5	ceramide synthase 5
CERS6	ceramide synthase 6
DES	desaturases
DMEM	Dulbecco's Modified Eagle Medium
DMSO	dimethyl sulfoxide
DNA	deoxyribonucleic acid
dNTP	dinucleotide triphosphates
EC	endothelial cell
FALDH	fatty aldehyde dehydrogenases
FCS	fetal cow serum
HMBS	hydroxymethylbilane synthase
GSL	glycosphingolipids
HCl	hydrochloric acid
HOCl	hypochlorous acid
JAM	junctional adhesion molecule
LPA	lysophosphatidic acid
MMP	matrix metalloproteinase

MPO	myeloperoxidase
mRNA	messenger RNA
MS	multiple sclerosis
N-cadherin	neural cadherin
OD	optical density
pBCEC	porcine brain capillary endothelial cells
VE-cadherin	vascular endothelial cadherin

List of figures

List of tables

Zusammenfassung

Ziel dieser Studie war es, ausgewählte Genprodukte des Sphingolipid (SL)-Metabolismus in primären mikrovaskulären Endothelzellen des Schweinehirns (pBMVEC) – der morphologischen Grundlage der Blut-Hirn-Schranke (BBB) – zu identifizieren. SLs behalten die BBB-Funktion durch Struktur und Signaleingabe bei. In einem ersten Schritt testete ich Primer für Enzyme, die am SL-Umsatz beteiligt sind, in RT-PCR- und RT-qPCR-Reaktionen. Ich habe auch untersucht, ob 2-Chlorhexadecanal (2-ClHDA), ein von Myeloperoxidase (MPO) abgeleiteter chlorierter Fettaldehyd, die Expression dieser Gene reguliert.

Hintergrund: Die neurovaskuläre Einheit (NVU) trennt das Gehirn vom Kreislauf und reguliert die neuronale Mikroumgebung. Die zerebralen Mikrogefäße sind empfindlich gegenüber oxidativem Stress (d. h. aberranter Redoxkontrolle). Oxidative Prozesse können die Integrität der NVU verändern und sind an den pathophysiologischen Vorgängen neurodegenerativer Erkrankungen beteiligt. Die Phagozyten-Hämperoxidase, MPO wandelt H_2O_2 in der Gegenwart von Chloridionen (Cl^-) in das starke Oxidationsmittel Hypochlorsäure (HOCl) um. HOCl kann Makromoleküle angreifen und sie modifizieren, wodurch eine Reihe von chlorierten Produkten erzeugt wird, die dem Wirt Gewebe- bzw. Organschäden zufügen können.

Methoden: Aus pBMVEC isolierte RNA wurden revers in komplementäre DNA von Enzymen transkribiert, die am SL-Metabolismus beteiligt sind. Die cDNA wurden in PCR- und quantitativen Echtzeit-PCR (qPCR) -Analysen verwendet. In einer ersten Reihe von Experimenten wurde die Primereffizienz analysiert. Anschließend untersuchte ich, ob 2-ClHDA die Transkription dieser Gene reguliert. Zellkulturen von pBMVEC wurden in Abwesenheit bzw. Gegenwart von 2-ClHDA inkubiert und Veränderungen in der Genexpression analysiert.

Ergebnisse: Die PCR-Bedingungen für den folgenden Satz von Genen, die an der SL-Synthese / dem SL-Abbau beteiligt sind, wurden festgelegt: Serin-Palmitoyltransferase 1, Serin-Palmitoyltransferase 2, Ceramidsynthase 5, Ceramidsynthase 6, Sphingomyelinsynthase 2, Sphingosinkinase 2, alkalische Ceramidase 1, alkalische Ceramidase 2, alkalisch Ceramidase 3, neutrale Ceramidase 2, Sphingomyelinphosphodiesterase, Sphingosin-1-phosphatphosphatase 1 und Sphingosin-1-phosphatlyase 1. In Reaktion auf

2-ClHDA wurde die Expression von CerS1, CerS6, SPHK2 bzw. SGPL1 hochreguliert.

Fazit: Die während der vorliegenden Pilotstudie erhaltenen Ergebnisse zeigen die Expression von Genen, von denen bekannt ist, dass sie an der SL-Homöostase beteiligt sind. Darüber hinaus legen meine Daten nahe, dass MPO-abgeleitetes 2-ClHDA das Potenzial hat, die SL-Biosynthesewege in pBMVEC zu stören.

Abstract

Aims of the study: This study aimed to identify selected gene products of sphingolipid (SL) metabolism in primary porcine brain microvascular endothelial cells (pBMVEC) – the morphological basis of the blood-brain barrier (BBB). SLs maintain BBB function by structural and signaling input. In a first step, I tested primers for enzymes involved in SL turnover in subsequent conventional RT-PCR and RT-qPCR reactions. I also tested whether 2-chlorohexadecanal (2-ClHDA) – a myeloperoxidase-derived chlorinated fatty aldehyde – regulates the expression of these genes.

Background: The neurovascular unit (NVU) separates the brain from peripheral circulation and regulates the neuronal microenvironment. The cerebral microvessels are sensitive to oxidative stress (i.e., aberrant redox control). Oxidative processes can alter the integrity of the NVU and are implicated in the pathophysiological sequelae of neurodegenerative diseases. The phagocyte heme peroxidase, myeloperoxidase (MPO) converts H_2O_2 into the strong oxidant hypochlorous acid (HOCl) in the presence of chloride ions (Cl^-). HOCl can attack and modify macromolecules generating a series of chlorinated products that can inflict tissue/organ damage on the host.

Methods: RNA isolated from pBMVEC was reverse transcribed into complementary DNA of enzymes involved in SL metabolism. The cDNA was used in PCR and real time quantitative PCR (qPCR) analyses and in a first set of experiments primer efficiency was analyzed. I then went on to assess whether 2-ClHDA regulates the transcription of these genes. Cell cultures of pBMVEC were incubated in the absence or presence of 2-ClHDA and changes in gene expression were analyzed.

Results: PCR conditions for the following set of genes involved in SL synthesis/degradation were established: serine palmitoyltransferase 1, serine palmitoyltransferase 2, ceramide synthase 5, ceramide synthase 6, sphingomyelin synthase 2, sphingosine kinase 2, alkaline ceramidase 1, alkaline ceramidase 2, alkaline ceramidase 3, neutral ceramidase2, sphingomyelin phosphodiesterase, sphingosine-1-phosphate phosphatase 1, and sphingosine-1-phosphate lyase 1. In response to 2-ClHDA, expression of CerS1**,** CerS6, SPHK2, and SGPL1 were upregulated.

Conclusion: The results obtained during the present pilot study demonstrate the expression of genes known to be involved in SL homeostasis. In addition, my data suggest that MPO-derived 2-ClHDA has the potential to interfere with SL biosynthetic pathways in pBMVEC.

1 Introduction

1.1 The Blood-Brain-Barrier

The brain operates within a well-controlled environment separated from the milieu of peripheral circulation [1]. The mechanisms that control this environment are collectively referred to as the blood-brain barrier (BBB) [2]. Diseases of the central nervous system (CNS), such as stroke, brain tumors, traumatic injury, Alzheimer's disease (AD), or multiple sclerosis (MS) are typically accompanied by BBB dysfunction resulting in secondary damage to neurons [3]. Understanding the regulatory properties of the BBB is therefore critical to understanding and treating BBB dysfunction in CNS diseases. Cerebrovascular endothelial cells form tight and adherens junctions and also interact with other cell types (pericytes, astrocytic endfeet, perivascular macrophages) to build up the functional cerebrovasculature termed the neurovascular unit [4]. The formation of the BBB – a process termed barriergenesis – is the final step during development of the brain vascular system that is induced by the embryonic neural tube and occurs in three steps, namely: i) brain angiogenesis, ii) differentiation of the BBB, and iii) formation and maintenance of the mature BBB [5]. Each of these steps is subject to complex signaling pathways that facilitate vascular sprouting. These events lead to the induction of phenotypic changes of cerebral endothelial cells which are characterized by the formation of complex tight- and adherens junctions (TJ and AJ respectively) strands and the acquirement of a polarized cell phenotype. The interaction of cerebral endothelial cells with pericytes and astroglia cells induces the transformation of 'naked' endothelial vessels to an intact cerebrovasculature with mature BBB properties. It is generally accepted that the formation of TJ is the 'sine qua non' for the BBB of all vertebrates [6]. In addition, an elaborate system of asymmetrically expressed transport proteins and receptors at the apical and basolateral plasma membrane of cerebral endothelial cells takes a central biochemical gate-keeping function at the BBB [6, 7].

1.1.1 Tight- and adherens junctions:

Tight junctions - The junctional complex of cerebral endothelial cells consists of TJ and AJ with the TJ forming the most apical constituent of the junctional complex

(Fig. 1). TJ are responsible for regulating paracellular permeability and cell polarity, two properties referred to as barrier and fence function. Integral proteins – occludin, claudins, and junctional adhesion molecule (JAM) – form the TJ in association with intracellular adapter/signaling proteins that link the TJ to the brain endothelial actin cytoskeleton [8]. Occludin was identified as the first integral membrane protein localized at TJ [9]. Although occludin colocalizes exclusively with TJ, studies from occludin-deficient mice revealed normal TJ formation in most tissues and suggested a fence function that contributes to asymmetrical protein distribution in brain capillary endothelial cells (BCEC) [10]. Claudins form a large family of proteins and in BCEC, claudin-5 (and to a lesser degree claudin-1 and -12) is most prominently expressed [11]. Studies from a claudin-$5^{-/-}$ mouse revealed that these animals develop a size-selective loosening of the BBB for compounds with a molecular mass <800 Da [12] indicating a molecular sieve-like function. The family of JAMs is involved in cell-cell adhesion junctional assembly of endothelial cells [13] and in Ca^{2+}-dependent transmigration of leukocytes across endothelial cells [14]. The TJ complex contains several intracellular accessory proteins termed zonula occludens proteins – ZO-1, -2, and –3; members of the membrane-associated guanylate kinase homolog – that function as recognition proteins for junctional placement, connection to the actin cytoskeleton and platforms for signaling proteins (reviewed in [7, 15]).

Adherens junctions - AJ are located closer to the basolateral side of BCEC, are formed by transmembrane adhesion molecules of the cadherin family that mediate homophilic cell adhesion and are also organized in multimeric complexes [15]. The core complex includes cadherin, beta-catenin bound to the cytoplasmic domain of cadherin, and α-catenin bound to the N-terminus of β-catenin. The integrity of this core complex is critical to the formation of AJ and is regulated by phosphorylation/dephosphorylation events [16]. Vascular endothelial cadherin (VE-cadherin) is a single-pass transmembrane protein that dimerizes laterally in *cis* and makes head-to-head contacts in *trans*. In addition to VE-cadherin, endothelial cells express neural cadherin (N-cadherin), which promotes endothelial cell (EC) adhesion and facilitates communication with other cell types (‘mural’ cells like pericytes, astrocytes, or smooth muscle cells). N-cadherin is clustered at the

basal membrane of EC, which are in tight contact with astrocytic endfeet and pericytes [17].

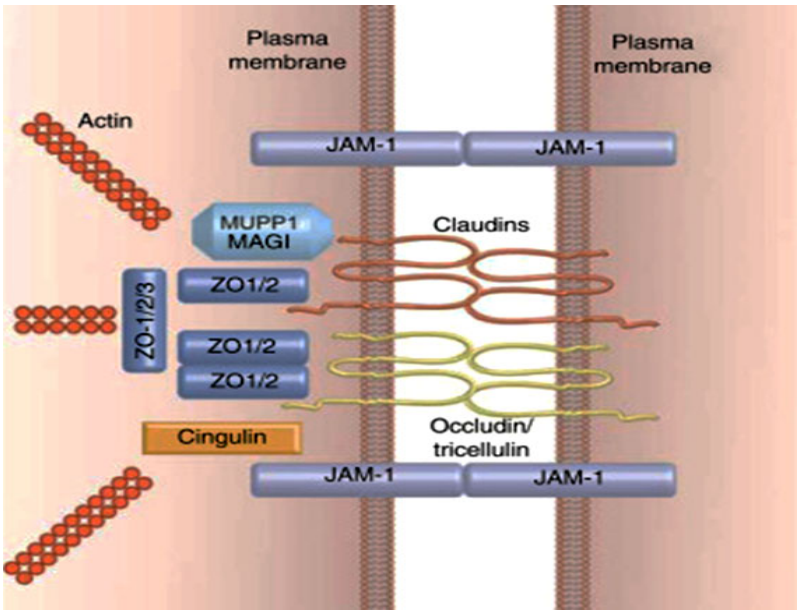

Fig. 1: Molecular interactions at tight junctions.
Lateral association of claudins (cis-interaction) results in the formation of oligomers whereas association of claudins on opposing membranes (trans-interaction) results in tight junction formation. Adopted from Ref. [18].

1.1.2 Transport of molecules across the BBB

Lipid soluble substances readily diffuse through the cerebral endothelial plasma membranes [19]. Transport of hydrophilic substances is either carrier-mediated, receptor-mediated, caveolae-mediated, or transporter-mediated (**Fig. 2**; [20]).

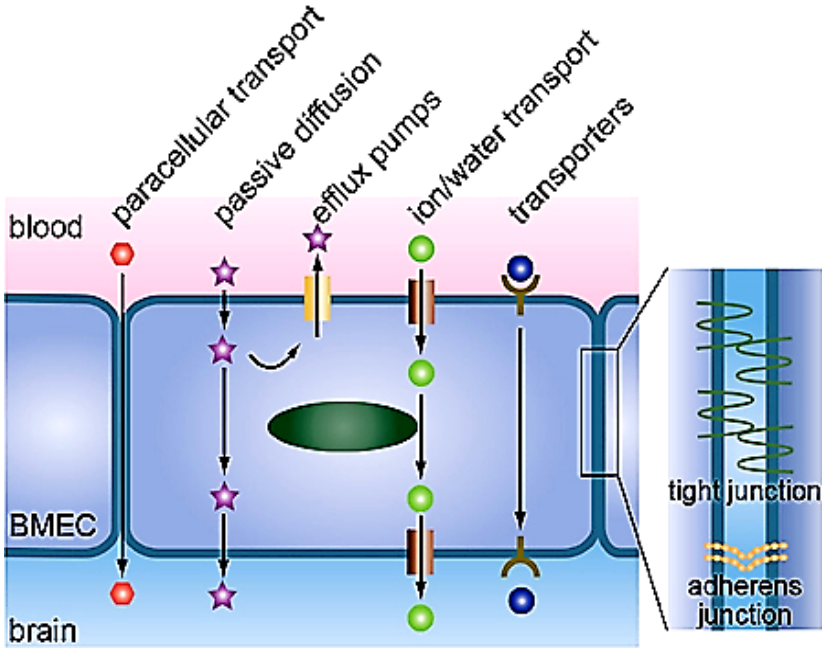

Fig. 2: Schematic illustration of transport routes across brain microvascular endothelial cells. Adopted from Ref. [19].

1.2 Sphingolipids are structural and signaling constituents of the BBB

Sphingolipids (SL) constitute a class of lipids defined by their eighteen-carbon amino-alcohol backbones, which are synthesized in the endoplasmic reticulum (ER) from non-SL precursors. Modifications of these basic structures are the basis of the vast family of sphingolipids that play significant roles in membrane biology and provide many bioactive metabolites that regulate cell function [21].

1.2.1 Biosynthetic pathways

SL are indispensable structural and signaling components, therefore aberrant SL homeostasis results in BBB dysfunction [22].

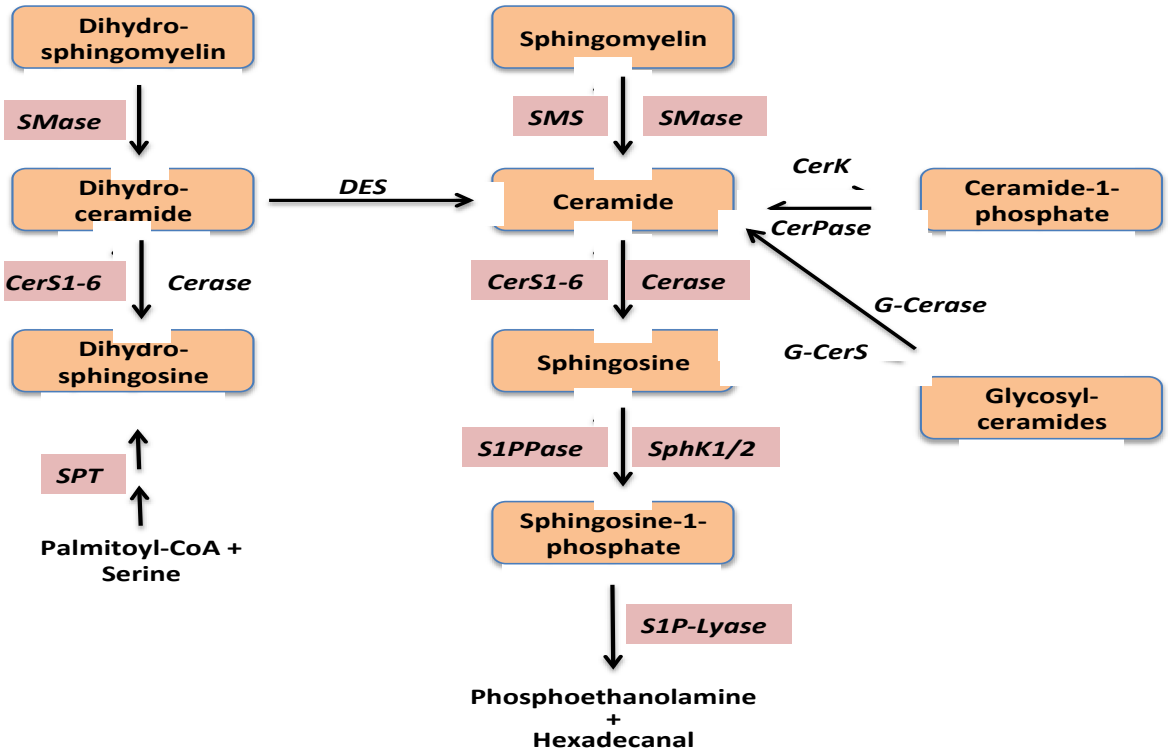

Fig. 3: Sphingolipids (SL) are potent regulators of a variety of biological programs impacting BBB function.
De novo synthesis starts in the ER where serine-palmitoyltransferase (SPT) catalyzes the condensation of C16-CoA and serine. A sequence of reactions involving ceramide synthases (CerS1-6) and desaturases (DES) leads to the formation of ceramide that can be converted to ceramide-1-phosphate (C1P) via ceramide kinase (CerK), complex glycosphingolipids (GSL) via glycosyl ceramide synthases (G-CerS), or sphingomyelin (SM) by sphingomyelin synthase (SMS). Hydrolysis of C1P, GSL, or SM generates Cer via the Salvage pathway. De-acylation of Cer (Ceramidase; Cerase) produces sphingosine, the precursor of sphingosine-1-phosphate (S1P) that is formed by sphingosine kinase-1 or -2 (SphK1/2). Hydrolysis of S1P by S1P lyase represents the irreversible exit point of this reaction sequence. Gene members subject to PCR analyses in the present study are shown in pink.

SL synthesis starts in the ER, where serine palmitoyltransferase (SPT) catalyzes the decarboxylation of palmitoyl-CoA and condensation with serine generating 3-ketosphinganine. This metabolite is then converted to dihydro-sphingosine, dihydro-ceramide, and finally ceramide via desaturases (DES) and ceramide synthases (CerS1-6). In the Golgi, ceramide is the precursor for sphingomyelin (SM) synthesis by SM-synthases (SMS). The SL rheostat is regulated by sphingosine kinases (SPHK1 and -2), which phosphorylate sphingosine to produce sphingosine-1-phosphate (S1P) (**Fig. 3**; Ref. [23]). S1P is secreted and serves as a signaling active lysophospholipid via one of the five cognate S1P receptors (S1PR1-5; Ref. [24]). S1PR1 plays a critical role in the maintenance of BBB function [25]. Disruption of SL homeostasis is commonly associated with endothelial barrier dysfunction and is often observed under septic conditions or in sepsis-associated encephalopathy [22].

1.2.2 Structures

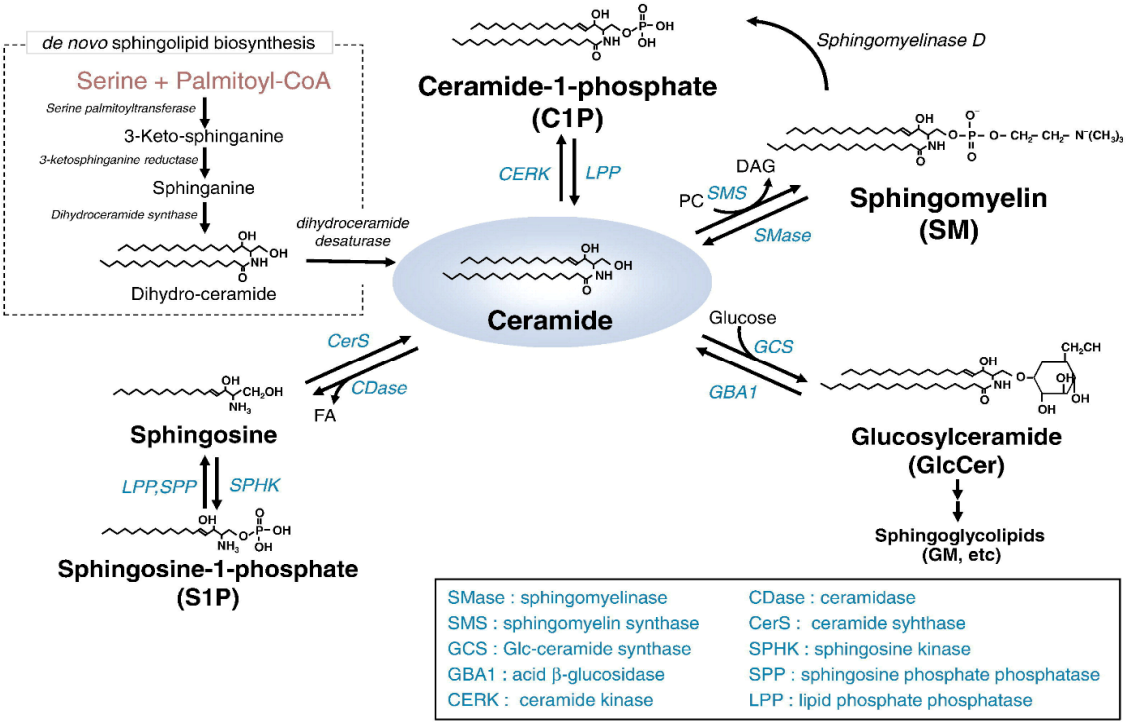

Fig. 4: Chemical structures of the different members of the SL family.
Adopted from Ref. [26].

Glycosphingolipids (GSL) are dozens of different sphingolipid species differing by both the order and type of sugar residues attached to their headgroup [26]. Another family is constituted by the sphingomyelin species, which are defined by a phosphocholine headgroup. A turnover scheme of the SL rheostat displaying basic chemical structures of the different classes is shown in **Fig. 4**.

1.2.3 Compartmentalization

Sphingosine and dihydrosphingosine are sufficiently amphipathic to diffuse between membranes and to flip between membrane leaflets; however, they also are likely to accumulate in acidic pH organelles due to ionization of their free amino group. Ceramide is likely to be restricted to the organelle in which it was created but may have access to enzymes or binding proteins on either side of the bilayer in which it was produced. Sphingomyelins and glycosphingolipids are mostly restricted to the luminal Golgi leaflet or on the outer leaflet of the plasma membrane after vesicular transport to that location. Sphingosine-1-phosphate (S1P) and dihydrosphingosine-1-phosphate (DHS1P) are also restricted to the hydrophilic compartments in which they are generated but can either be exported to the extracellular space with the aid of specific transporters or be dephosphorylated into a more hydrophobic compound [27, 28].

1.2.4 The BBB is under attack in inflammatory and neurological diseases

Under conditions of oxidative stress – i.e. an imbalance of pro- and antioxidants – macromolecular damage can occur [29]. This pathway was identified in peripheral, cardiovascular, metabolic, and neurological pathologies. Of note, oxidative stress appears to be a common denominator in barrier dysfunction frequently observed in neurological disorders [30]. A loss of barrier integrity permits the entry of plasma components, red blood cells, and leukocytes into the brain. Neurotoxic products are generated, which can compromise synaptic and neuronal functions [31].

1.2.5 Oxidative attack

The immune system is able to produce free radicals, such as reactive oxygen species (ROS) or nitric oxide (NO), which protect the host but under chronic activation can also induce host tissue damage [32]. In healthy conditions, ROS are scavenged by endogenous antioxidants, e.g. superoxide dismutase or glutathione peroxidase. However, pathological conditions such as ischemia and chronic inflammation can cause overshooting ROS production, which can overwhelm the defense mechanism. This is commonly described as oxidative stress [33]. Polyunsaturated lipids/fatty acids after reacting with ROS can become oxidized, destroying the structure of myelin and cell membranes. Exposure of endothelial

cells to ROS can threaten the integrity of the BBB both directly (e.g., by downregulating the synthesis of proteins involved in tight junctions between cells) and/or by activation of matrix metalloproteinases (MMP) [34].

1.2.6 Myeloperoxidase (MPO)

MPO is a heme peroxidase that catalyzes the reaction between H_2O_2 and chloride ions to produce HOCl as the primary oxidant. This is important in antimicrobial activities of the innate immune system. However, MPO-derived oxidants are also implicated in inflammatory diseases, such as atherosclerosis, multiple sclerosis, Parkinson's, or Alzheimer's disease [35].

1.2.7 Reactive aldehydes

Aldehydes can diffuse through cell membranes and form adducts with macromolecules, thereby usually modulating or disrupting their function [36]. Reactive aldehydes are readily formed during oxidative stress as products of lipid peroxidation [37]. Therefore, a mechanism for rapid clearance of these highly diffusible and harmful aldehydes is crucial to protect cells and tissues from damage. Increasing the catalytic activity of aldehyde dehydrogenase 2 (ALDH2) may provide a novel and effective means to reduce oxidative stress induced cell- and organ dysfunction and therefore support human health [38].

1.2.8 MPO generates plasmalogen-derived reactive chlorinated aldehydes in vitro and in vivo

Plasmalogens constitute ~ 15–20% of total phospholipids in cell membranes [39]. The hydrogen atoms adjacent to the vinyl ether bond of plasmalogens have relatively low dissociation energies and are preferentially oxidized over diacylglycerophospholipids when exposed to free radicals [40]. Plasmalogens are consumed in this reaction. This was proposed to spare the oxidation of other vulnerable membrane lipids. However, it remains to be determined whether the oxidative products themselves might be harmful, and these include free aldehydes, 1-hydroxy (or lyso)-2-acyl-sn-GP, 1- formyl-2-acyl-sn-GP, allelic hydroperoxides, epoxides and hemiacetals [41].

The vinylether bond of plasmalogens is also targeted by MPO-derived HOCl resulting in the generation of chlorinated aldehydes (prototypic member is 2-

ClHDA) and the corresponding lyso-phospholipid. This process occurs in vitro as well as in vivo and damages brain endothelial cell- and BBB function [42]. 2-ClHDA is subject to further metabolism by fatty aldehyde dehydrogenases (FALDH) and the generated chlorinated fatty acid can undergo consecutive ω- and subsequent β-oxidation [43, 44]. Following headgroup hydrolysis of lyso-phosphatidylethanolamine by autotaxin (ATX), lysophosphatidic acid (LPA) is generated. These steps are summarized in **Fig. 5**.

Evidence coming from pre-clinical rodent models and from human patient support the association of MPO and its cytotoxic product, hypochlorous acid (HOCl) in neurodegenerative diseases including Alzheimer's disease, Parkinson's disease, amyotrophic lateral sclerosis, multiple sclerosis, stroke, or epilepsy [45].

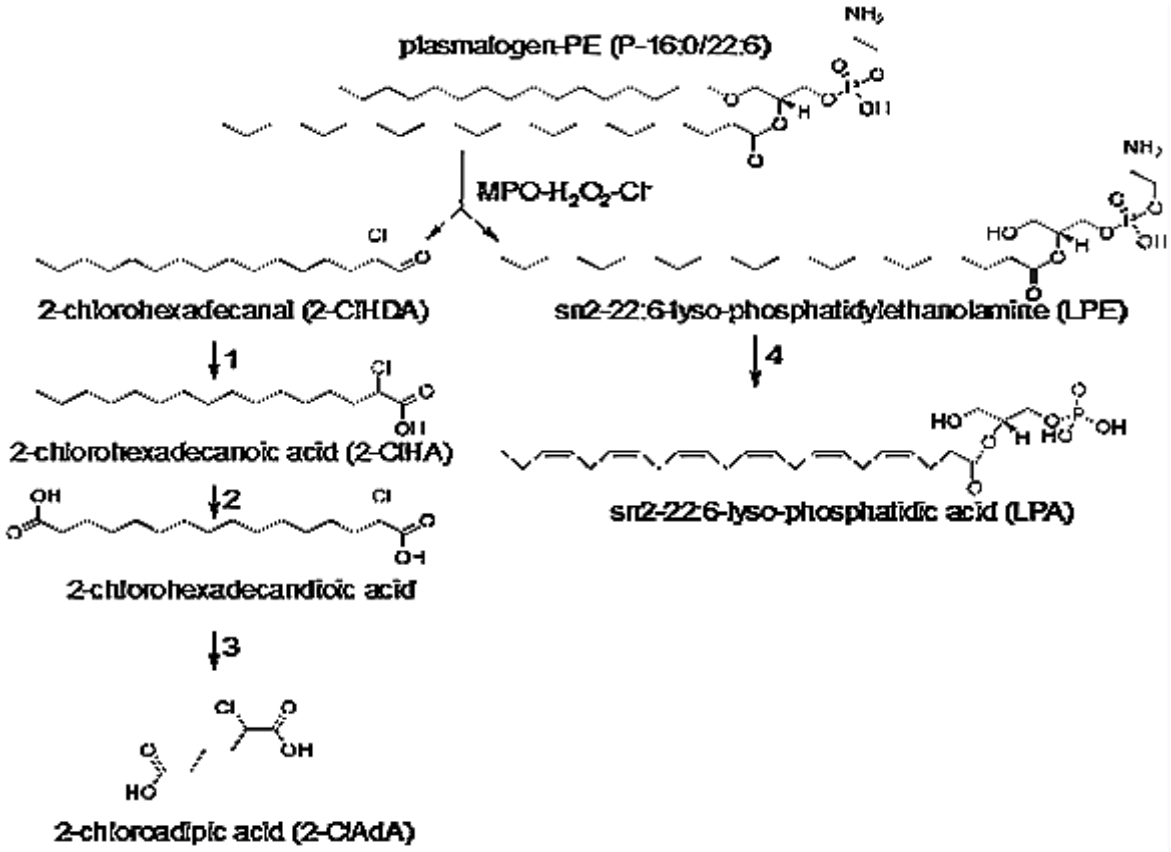

Fig. 5: Modification of the P-16:0/22:6 plasmalogen-phosphatidylethanolamine (PE) Species

Enzymatic pathways involved are given in numerical order: 1 = fatty aldehyde dehydrogenase, 2 = ω-oxidation, 3 = β-oxidation starting at the ω-C atom, 4 = autotaxin. Adopted from Ref. [46].

2 Materials and Methods

2.1 Aims of the study

Üllen et al. [46, 47, 48] have demonstrated that myeloperoxidase-derived oxidants induce blood-brain barrier (BBB) dysfunction with concomitant generation of 2-chlorohexadecanal.

The objectives of the present pilot study were to extend these findings and get first indications whether 2-ClHDA can act as a transcriptional regulator of SL synthesis in brain endothelial cells. Primary porcine microvascular brain endothelial cells (pBMVEC) were used as an in vitro model of the BBB.

In particular, the present pilot study aimed to:

1. Establish experimental conditions for RT-PCR and RT-qPCR analysis of a specific set of genes involved in SL turnover in pBMVEC, and,
2. Determine whether 2-chlorohexadecanal (2-ClHDA) – a reactive chlorinated aldehyde generated during inflammatory diseases – impacts expression levels of these RNAs in pBMVEC.

2.2 Materials

2.2.1 Chemicals

- 2-chlorohexadecal synthesized as described by Üllen et al [49].
- Dimethyl sulfoxide (DMSO)
- 2-Mercaptoethanol

2.2.2 Glassware and plastics

- Disposable pipettes and plastic pipette tips
- Disposable cell scrapers, Greiner bio-one, Austria
- Cell culture flasks (75 cm^2), Sigma Aldrich
- 6-well cell culture plates
- Eppendorf® micro test tubes (200 µl, 500 µl, 1 ml), Eppendorf, Germany
- Nuclease free microcentrifuge tubes

2.2.3 Lysis solution A:

- 0.04 M HCl in absolute isopropanol (= 1M HCl/isopropanol 1:25, v/v); kept at -70 °C.

2.2.4 Cell Culture Medium

- Collagen 150 µg/ml
- Medium A: serum free
- Medium 199 with L-glutamine, Gibco®, Scotland, UK
- Ascorbic acid
- Hydroxyethylpiperazine ethansulfonoat
- Lipid concentrate
- Hydrocortison
- Penicillin and Streptomycin
- Basic fibroblast growth factor (bFGF).
- Medium B: with serum
- Medium A
- Fetal calf serum (FCS Gold) 5%

2.2.5 Kits

- RNeasy® Plus Mini kit, QIAGEN
- QuantiTect SYBR® Green PCR Kits, QIAGEN
- SuperScript™ III Reverse Transcriptase, Invitrogen

2.2.6 Laboratory equipment

- Accu-Pipette, Eppendorf.
- Mastercycler, Eppendorf.
- Microcentrifuge, Eppendorf.
- Victor X3 Multilabel plate reader, PerkinElmer
- Spectrophotometer NanoDrop 1000, Thermo Scientific.
- ABI 7000 HT, Applied Biosystems.
- 1DTM imaging system, Kodak

2.3 Methods

2.3.1 Primary pBMVEC cultures as in vitro model of the BBB

PBMVEC were isolated from porcine brain samples, obtained from the local slaughterhouse, by a combination of sequential enzymatic digestion and centrifugation steps exactly as described by Üllen et al. [49]: After removal of meninges and the secretory areas, the brain cortex (gray and white matters) was minced using a sterile cutter with staggered rolling blades. Minced tissue was suspended in 'preparation medium' [M199 supplemented with penicillin/streptomycin (P/S;100mg/ml), gentamycin (100 mg/ml) and glutamine (0.68 mM)] and incubated with solid dispase (0.1% w/v) for 1 to 2 h at 37 °C in a water bath with gentle stirring. Dextran solution (16 %, w/v) was added to get a final 10% (w/v) dextran suspension followed by centrifugation at 6800 g for10 min at 41C. The resulting pellet was resuspended in 'Medium A' [M199 supplemented with P/S (100 mg/ml), gentamycin (100 mg/ml), and glutamine (0.68mM and 10 % ox serum)]. Larger vessels were separated by a filtration through a 180-mm nylon mesh. Microvessels were digested with 0.03 % (w/v) collagenase/dispase for 5 min at 37 °C in a water bath with gentle stirring. Released PBCEC aggregates were collected by low-spin centrifugation at 140 g for 10 min at room temperature (RT) and further purified by density gradient centrifugation. Cells obtained from one brain were resuspended in 5 ml medium A and centrifuged on a discontinuous Percoll gradient (20 ml 1.03g/ml bottom-layered with 15 ml 1.07 g/ml) at 1300 g for 10 min at RT in a swing-bucket rotor without brake. BMVEC clusters, which were gathered at the interface of the two phases, were washed in medium A and plated onto six to eight 75 cm² collagen-coated culture flasks. After 1 day in culture, the cells were washed twice with phosphate-buffered saline (PBS) and cultivated in ''medium B'' (medium A without gentamycin). After 2 to 3 days, when confluence was almost reached, pBMVEC were subcultured by trypsinization and seeding onto collagen-coated cell culture ware (60 mg/ml collagen in PBS).

2.3.2 Harvesting of cells

PBMVEC were harvested according to instructions in the manufacturer's handbook of RNeasy® Plus Mini kit [50]. The culture medium was completely aspirated, and the cells were washed twice with 10 ml ice cold PBS. The cells

were directly lysed in the 6-well culture plates by adding a mixture of 3.5 µl β-mercaptoethanol and 350 µl RLT buffer (guanidine isothiocyanate) for RNA isolation.

2.3.3 RNA isolation

Cell lysis was immediately followed by isolation of RNA using RNeasy® Plus Mini kit. The cell lysates were transferred into QIAshredder columns and RNA was isolated following the manufacturer's protocol [50]. Isolated RNA was eluted in 30 µl RNase-free water. The concentrations of isolated RNA samples were measured with 1 µl of each RNA suspension using a NanoDrop® 1000.

2.3.4 Reverse Transcription

RNA samples were used to synthesize their complementary DNA (cDNA) following the manufacturer's instructions for SuperScript™ III Reverse Transcriptase (Invitrogen; [51]). The following components were added to a nuclease-free microcentrifuge tube for each 20 µl reaction: 3 µg of total RNA (1 ng – 5 µg according to manufacturer), 1 µl (100µM) 50-250 ng random hexamers (Thermo Scientific), 1 µl dNTP Mix (10 mM) each, 3 µg total RNA (3000 ng; 771.3 ng/µl), varying amounts of sterile distilled water for a total volume of 12 µl. The mixture was briefly vortexed and heated for 5 min at 65°C. The setups were incubated for at least 1 minute on ice and vortexed, before the following components were added: 4 µl 5X First-Strand Buffer, 2 µl 0.1 M DTT, 1 µl sterile distilled water and 1 µl (200 units) of SuperScript™ III Reverse Transcriptase. The contents of each tube were gently mixed and after centrifugation, the mixture was incubated in a thermocycler at 25°C for 2 min. 1 µl (200 units) of SuperScript™ III Reverse Transcriptase was then added. The reaction was incubated at 50°C for 50 min and terminated by incubating at 70°C for 15 min. Before PCR, 10 µl distilled water was added to the cDNA.

2.3.5 Polymerase chain reaction (PCR)

PCR was carried out using DreamTaq™ DNA polymerase according to the manufacturer's instructions [52]. For each 20 µl reaction, 4 µl 5X PCR Buffer [200 mM Tris-HCl (pH 8.4)], 0.4 µl 25 mM dinucleotide triphosphates (dNTP) mix, 1 µl of a mixture of forward and reverse primers (each having a final concentration of

10 µM), 0.2 µl DreamTaq™ DNA polymerase (5 U/µl), 2 µl cDNA of a 1:50 dilution, and sterile water was added to a final volume of 20µl. The mixture was briefly centrifuged and incubated in a thermal cycler for one cycle at 95 °C for 2 minutes. The PCR was performed at 95 °C for 30 seconds, 57 °C for 30 seconds and elongation at 72 °C for 1 minute, for 40 cycles. The reaction was incubated at 72 °C for 10 minutes and then maintained at 4 °C before being stored at -20 °C.

Table 1: Genes of sphingolipid metabolism amplified by conventional reverse transcription-polymerase chain reaction (RT-PCR)

name of primer-pair* (primers)	**Oligo name**	**Name and (NM_number)**	**Name of protein and (NP_number)**
SS1	hs_SPTLC2	serine palmitoyltransferase, long chain base subunit 2 (NM_004863.3)	serine palmitoyltransferase, 2 (NP_004854.1)
SS6	hsSPTLC1B	serine palmitoyltransferase, long chain base subunit 1 (NM_004863.3)	serine palmitoyltransferase, long chain base subunit 1 (NP_001268232).
SS8	hsSGPL1	sphingosine-1 -phosphate lyase 1 (NM_003901.3)	sphingosine-1-phosphate lyase 1 (NP_003892)
SS9			
SS13	hsACER2	alakline ceramidase 2	alkaline ceramidase 2 (NP_001010887)

name of primer-pair* (primers)	**Oligo name**	**Name and (NM_number)**	**Name of protein and (NP_number)**
SS14	hs_ACER3	Alkaline ceramidase 3 (NM_018367.6)	alkaline ceramidase 3 (NP_001287884)
SS21	hsCERS5	ceramide synthase 5 (NM_147190	ceramide synthase 5 (NP_001268660.1)
SS22	hsCERS6	Ceramide synthase 6 (NM_001256126.1)	ceramide synthase 6 (NP_001243055.1)
SS23			
SS26	hs_SGMS2	Sphingomyelin synthase 2 (NM_152621.5)	sphingomyelin synthase 2 (NP_689834.1)
SS32	pSPHK2	sphingosine kinase 2 (NM_020126)	sphingosine kinase 2 (NP_001191087.1)
SS33	782 rev, pSGPP1	Sphingosine-1 -phosphate phosphatase (NM_030791)	Sphingosine-1-phosphate phosphatase (XP_013839990)

Table 2: Primers used for amplification by conventional RT-PCR

name of primer-pair* (primers)	Name of primer	Position and Oligo name	Primer pair	size of PCR product (bp)	Oligo sequence (5' to 3')
SS1	S25	315f, hsSPTLC2	S25/S26	869	GGCCAGATCCATCATGTTAC
	S26	1183rev, hs_SPTLC2			GCAATCACTTCAGGAAGACG
SS6	S34	758, hsSPTLC1B	S32/S34	689	GCATGTTGGCCAGGCTGGTT
SS8	S36	230f, hsSGPL1	S36/S37	837	GCACAGACCTTCTGATGTTG
	S37	1066rev, hsSGPL1			TGGCAGTGTTCCTGGAGATA
SS9	S38	776rev, hsSGPL1	S36/S38	547	TCTATCTTGCGTAGTCCTGG
SS13	S44	243f, hsACER2	S44/S45	633	GCTATCGCCGAGTTCTACAA
	S45	875rev, hs_ACER2			AGGAATCTCTGAGGCAGCAT
SS14	S46	198f, hsACER3	S46/S47	596	GCCGAGTTCTGGAATACAGT
	S47	793rev, hs_ACER3			AGATAGGAACCAAGGCCAGT
SS21	S57	241f, hsCERS5	S57/S58	540	GTATTGGCATCGAGGACAGT
	S58	780rev, hs_CERS5			CCAGCAAGAAGTCTGAGACA
SS22	S59	137f, hsCERS6	S59/S60	629	TTAGCCTGGTTCTGGAACGA
	S60	765rev hsCERS6			ACAAGGTGGTGCAGGAACAT
SS23	S61	191f, hsCERS6	S61/S60	575	GACCTGAAGAACACGGAGGA
SS26	S66	636f, hsSGMS2	S66/S67	514	CGCTGAACCTGTTGAAGAAG
	S67	1149rev, hs_SGMS2			TGCCTGAGAGTCTCCATTGA
SS32	S7	f, pSPHK2	S7/S8	947	ATAAGGAGCTGAAGGCAGGA
	S8	r, pSPHK2			TGCAGTTGGTCAGGAGGTCT
SS33	S11	467f, pSGPP1	S11/S14	315	AACTGGCCGCTCTACTACCT
	S14	782 rev, pSGPP1			CTTCCATGTGCTGTCTTGCT
*primer-pair: 10 µl primer1+10 µl primer2 +20 µl water=25 µM					

2.3.6 Gel electrophoresis

1.2 % agarose gel was used to visualize PCR products. The gel was prepared by dissolving 4.8 g agarose in 400 ml 0.5x Tris/acetate/EDTA buffer (TAE). The solution was heated in a microwave to dissolve the agarose. After cooling down to 56 °C, ethidium bromide was added to the dissolved agarose and gently mixed. The gel was poured into an electrophoresis box fitted with two gel combs. After an hour, the combs were removed from the solidified gel, leaving behind wells for loading DNA samples. The gel was covered with 1000 ml running buffer (0.5 X TAE).

10 µl of each PCR product, as well as 3 µl of the DNA size marker Lambda Hind III / phiX Hae III, were loaded into respective wells. Electrophoresis was carried out at 75 V for 60 min. Afterwards, the gel was photographed under UV light on a Kodak 1DTM imaging system.

2.3.7 Treatment with 2-ClHDA

Cells were incubated in 6-well culture plates in serum-supplemented culture medium up to confluence. The medium was then completely removed and replaced with serum-free culture medium. After 12 hours, cell cultures were treated with 15 µM 2-ClHDA [diluted with dimethyl sulfoxide (DMSO)] for 1, 3, 5 and 12 (i.e. overnight) hours. DMSO served as vehicle control.

Cell lysis, isolation of RNA and reverse transcription were carried out as previously described.

2.3.8 Real time quantitative PCR (RTqPCR) with SYBR® Green Dye

Quantitative PCR was performed using LightCycler (Applied Biosystems) and QuantiFast SYBR® Green RT-PCR kit according to manufacturer's protocol [53].

Each setup contained 1 µl primer (assays for human genes), 4 µl cDNA (diluted in RNase-free water), 5 µl SYBR® Green PCR Master Mix (containing: HotStar Taq DNA Polymerase, SYBR® Green I dye, ROX dye, dNTP mix with dUTP and Quantitect SYBR Green PCR buffer).

To find the optimum concentration of cDNA samples to be used in qPCR, different dilutions of the samples (1:10, 1:20, 1:50, 1:100 and 1:200) were used in an initial run. The dilution 1:100 proved favorable and was used in subsequent runs.

Table 3: QuantiTect primer assays (Qiagen) that were used for RT-qPCR experiments.

Primer	Name of Enzyme	QT number
SPHK2	Sphingosine kinase 2	QT00085386
ACER1	Alkaline ceramidase 1	QT00049000
ACER2	Alkaline ceramidase 2	QT00009191
ASAH2	N-Acylsphingosine amidohydrolase	QT01335264
CERS5	Ceramide synthase 5	QT00032130
CERS6	Ceramide synthase 6	QT00076118
SPTSS	Serine Palmitoyltransferase, Small Subunit A	QT00038311

The housekeeping gene hydroxymethylbilane synthase (HMBS) served as the reference gene for normalizing the target gene expression. The enzyme plays a vital role in the synthesis of heme, which is an essential component of hemeproteins, e.g., hemoglobin.

2.3.9 Statistical analysis of data

Mean crossing point (C_P) values obtained through qPCR were statistically analyzed with the gene quantification software Relative Expression Software Tool (REST® 384; [54]).

Standard curves for the calculation of qPCR efficiency were established in GraphPad Prism 5.0a and subjected to linear regression analysis. The calculated slopes ('k') were used to calculate qPCR efficiency ($E = 10^{(-1/k)}-1$) using an open-source analysis tool from Horizon Discovery [55].

3 Results

3.1 RNA isolation from untreated and 2-ClHDA-treated pBMVEC

Optical densities (OD) of isolated RNA were measured at wavelengths 280 nm, 260 nm and 230 nm. The ratio OD260/OD280 is a measure for contamination by proteins and the ratio OD260/OD230 for contamination by other compounds. As can be seen from **Table 4**, the isolation protocol was optimized to give OD260/OD280 ratios of >2, which is an indication of a highly 'pure' (i.e. only low protein content) RNA.

The OD260/OD230 ratio is indicative for the presence of organic compounds including phenol, Trizol, salts (chaotropic), or aromatic compounds. Samples with OD260/OD230 ratios below 1.8 are considered to be contaminated and in reverse transcription this ratio should be ≥ 2. Thus, all of my RNA preparations fulfilled the quality requirements for reverse transcription.

Table 4: Yields and optical density ratios of RNA samples isolated from untreated pBMVEC.

Sample ID	ng/µl	OD260/OD280	OD260/OD230
1	569.1	2.13	2.08
2	521.26	2.16	2.13
3	510.83	2.17	2.1
4	550.18	2.17	2.1

Table 5: Yields and optical density ratios of RNA samples isolated from 2-ClHDA-treated pBMVEC.

pBMVEC were treated with 2-ClHDA (1-5 µM) for the durations indicated, cells were washed, lysed and RNA was isolated. Optical densities were determined on a NanoDrop instrument.

Duration (h)	ng/µl	OD260/OD280	OD260/OD230
1	148.68	2.10	1.62
3	144.05	2.09	1.32
5	140.82	2.09	1.31
12	137.18	2.11	1.89

Data shown in **Table 5** revealed that RNA yields and purity were lower in 2-ClHDA-treated cells as compared to untreated cells. However, the reason for this observation is currently unclear.

3.2 Reverse transcription-polymerase chain reaction (RT-PCR)

In a first set of experiments, I converted RNA isolated from pBMVEC into cDNA by a reverse transcription (RT) reaction that was used as template for a polymerase chain reaction (PCR) to test for the presence of gene products involved in SL homeostasis. Primers were designed and directed against the human gene products. PCR products that were obtained with the primer pairs displayed in **Table 2** were separated on 1.2 % agarose gels and revealed the presence of transcripts in the expected size range. Lambda Hind III/phiX Hae III was used as DNA size marker. As can be seen from **Fig. 6** primers and PCR conditions were successfully established and (except for ACER1, CerS1, ASAH1 where I obtained no PCR products) yielded amplicons of the expected transcript size (compare **Table 2** and **Fig. 6**).

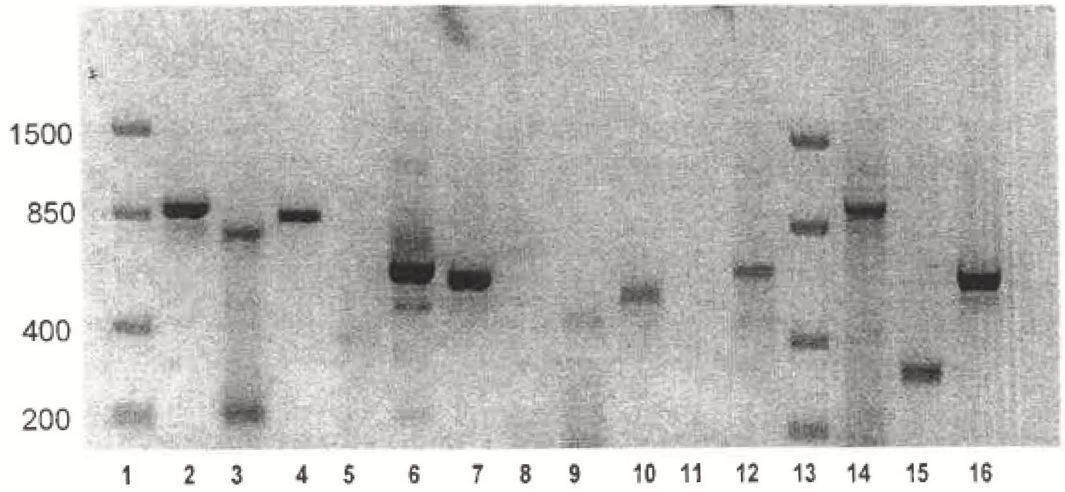

Fig. 6: Separation and visualization of RT-PCR products on 1.2 % agarose gels
10 µl of the PCR products were loaded on 1.2 % EtBr agarose gels and separated at 200 V (90 min). Photographs were taken on a Kodak 1DTM imaging system. Size of PCR products (kb) were estimated by comparison with the standards shown in lanes 1 and 13 representing the Lambda Hind III/phiX Hae III marker.
Lane assignment:
1= Std, 2 = SPTLC2 (primer pair S25/26, size 869 bp), 3 = SPTLC1B (primer pair S33/34; size = 689), 4 = SGPL1 (primer pair S36/37; size = 837), 5 = ACER1 (no product), 6 = ACER2 (primer pair S44/45; size 633), 7 = ACER3 (primer pair S46/47, size 596), 8 = CerS1 (no product), 9 = CerS5 (primer pair S57/58; size = 540), 10 = SMS2 (primer pair S66/67 size = 575), 11 = ASAH1 (no product), 12 = CerS6 (primer pair S59/60; size = 629), 13 = Std, 14 = SPHK2 (primer pair S7/8; size = 947), 15 = SGPP1 (primer pair S11/14; size = 315), 16 =SGPL1 (primer pair S22/23; size = 623). Primer sequences and NM numbering are shown in **Tables 1** and **2.**

3.3 Establishment of qPCR conditions and determination of qPCR efficiencies

qPCR is the most sensitive analytical method to quantify also low concentrations of nucleic acids and allows absolute and relative (normalization on a reference gene) quantification. To assess the quality of the qPCR conditions established here (for the target genes displayed in **Table 3**), I have set up calibration curves to determine PCR efficiency (the fraction of target molecules that are amplified within one cycle of the reaction [56]). As outlined by Svec and colleagues [56], PCR efficiency is determined by setting up serial dilutions of the target, running multiple PCR reactions, and plotting mean crossing point (C_P) values vs. log input to establish a calibration curve. Linear regression analysis is then used to calculate the slope of the calibration curve, a parameter needed to calculate efficiency (E) since $E = 10^{-(1/slope)} - 1$. From the C_P values displayed in **Table 6,** I have established calibration curves for the individual gene products analyzed (**Fig. 7**) and determined the corresponding slopes (k) using GraphPad Prism. Efficiencies were calculated using an open-source online tool [55]. Ideally, the efficiency of the assay should be 100% indicating that the target gene is doubling with each cycle. Perfect PCR efficiency will demonstrate a change of 3.3 cycles (the slope) between 10-fold dilutions of template. In real laboratory life, qPCR efficiency should be >90% (although it is possible to perform accurate measurements with assays exhibiting <90% efficiency).

During the present experiments, I have obtained efficiency values between 96 and 115 % (**Table 6**), where E>100 % are most likely due to inhibited amplification at high template concentrations, resulting in lower k-values and thus overestimation of the reaction efficiency.

Table 6: PCR efficiency estimated for the indicated gene products.

RNA from pBMVEC was reverse transcribed into cDNA. The cDNA was serially diluted and used for qPCR analyses for the indicated gene products. C_P values were plotted against logcDNA and the slope of the resulting calibration curves (r^2 is given below k-values) was calculated and used to determine qPCR efficiency.

Target gene	cDNA input [ng]	Mean Crossing Point (C_P)	Slope (k) r^2	Efficiency (%)
hHPRT	100	22.203	-3.337	99.4
	50	23.087		
	20	24.527	0.9986	
	10	25.495		

Target gene	cDNA input [ng]	Mean Crossing Point (C_P)	Slope (k) r^2	Efficiency (%)
SGMS2	100	22.073	-3,322 0.9988	100.0
	50	22.963		
	20	24.263		
	10	25.303		
	5	26.390		
SGPL1	100	22.740	-3,001 0.9961	115.4
	50	23.500		
	20	24.700		
	10	25.820		
	5	26.530		
SPTLC1	100	21.707	-3,264 0.9963	102.5
	50	22.480		
	20	23.760		
	10	24.827		
	5	25.927		
ACER1	100	31.937	-3,25 0.9888	103.1
	50	32.580		
	20	33.923		
	10	34.843		
	5	36.177		
ACER2	100	23.970	-3,239 0.9481	103.6
	50	24.827		
	20	26.977		
	5	28.013		
SPHK2	100	25.723	-3,282 0.9945	101.7
	50	26.723		
	20	27.960		
	10	29.230		
	5	29.883		
SMPD1	100	22.647	-3,107 0.9972	109.8
	50	23.383		
	20	24.675		
	10	25.610		
	5	26.663		
ASAH2	50	22.303	-3,418 0.9923	96.1
	20	23.497		
	10	24.463		
	5	25.760		
SPTSSA	50	26.420	-3,173 0.9986	106.6
	20	27.623		
	10	28.693		
	5	29.557		
SMPD3	50	30.790	-3,303 0.9764	100.8
	20	31.620		
	10	32.873		
	5	34.047		
SPTLC2	50	23.667	-3,003 0.9974	115.3
	20	24.777		
	10	25.650		
	5	26.690		

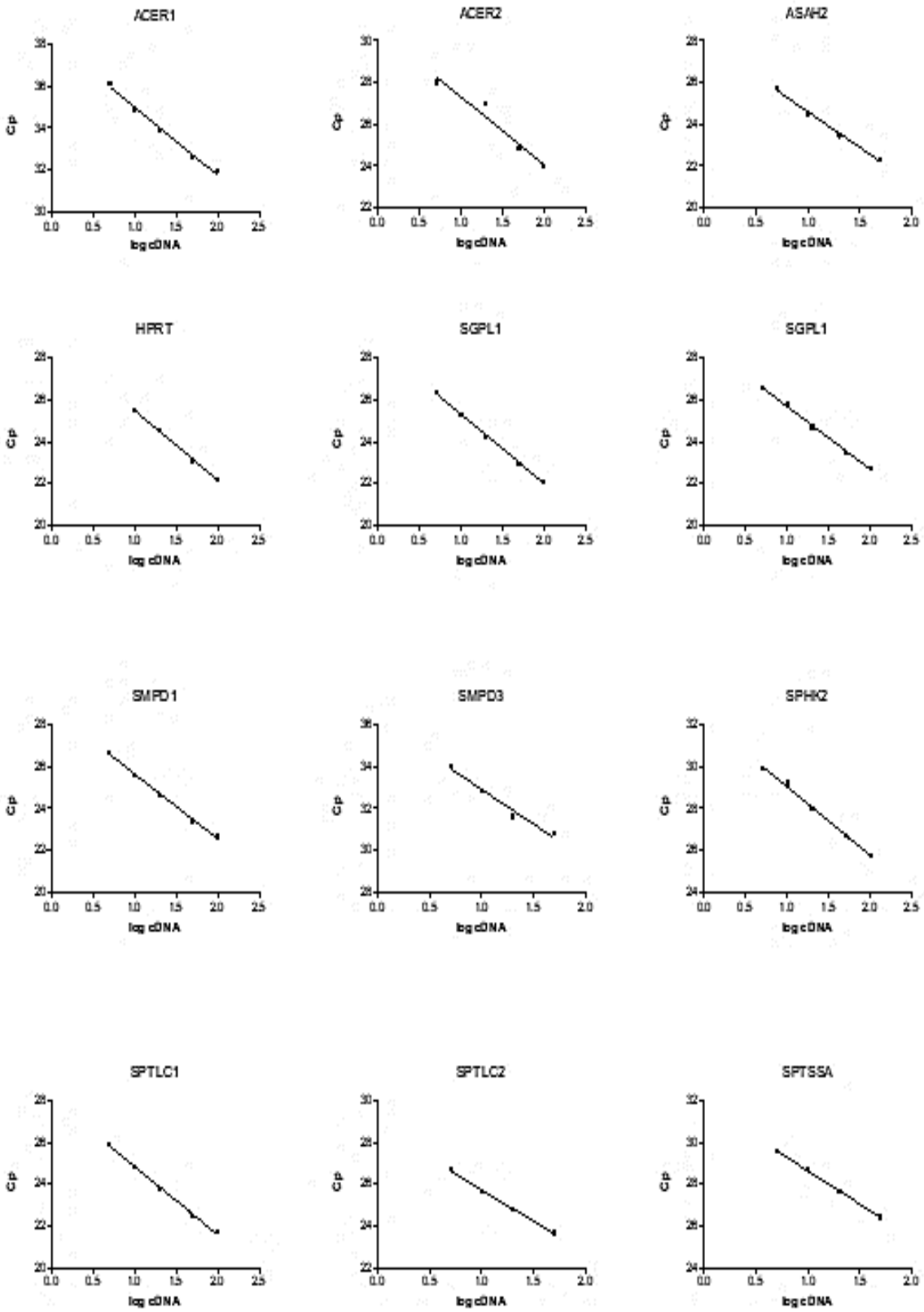

Fig. 7: Calibration curves for the target genes analyzed.
GraphPad Prism5.0a was used for linear regression analysis. The corresponding calculated slopes and r^2 values are displayed in **Table 5** and were used to calculate E using the open-source calculator from Horizon Discovery [55]. The Cp values shown represent mean values from three technical replicates.

3.4 2-ClHDA alters expression of gene products involved in sphingolipid metabolism of pBMVEC

Having established optimal conditions for qPCR analysis, I tested the effect of 2-ClHDA on the expression levels of these gene products. During these experiments, pBMVEC were kept serum-free overnight, were then incubated in the presence of 15 µM 2-ClHDA for the indicated periods, cells were washed, RNA was isolated, reverse transcribed and the target genes were analyzed by qPCR on a Light Cycler instrument. As can be seen from **Fig. 8**, expression of SPTLC2, SMS2, SMase and ceramidase was unaffected by the chlorinated aldehyde. In contrast, CerS1, CerS6, SPHK2, and S1PL were significantly upregulated by 2-ClHDA. Data presented in Fig. 8 are all normalized to HPRT as reference gene.

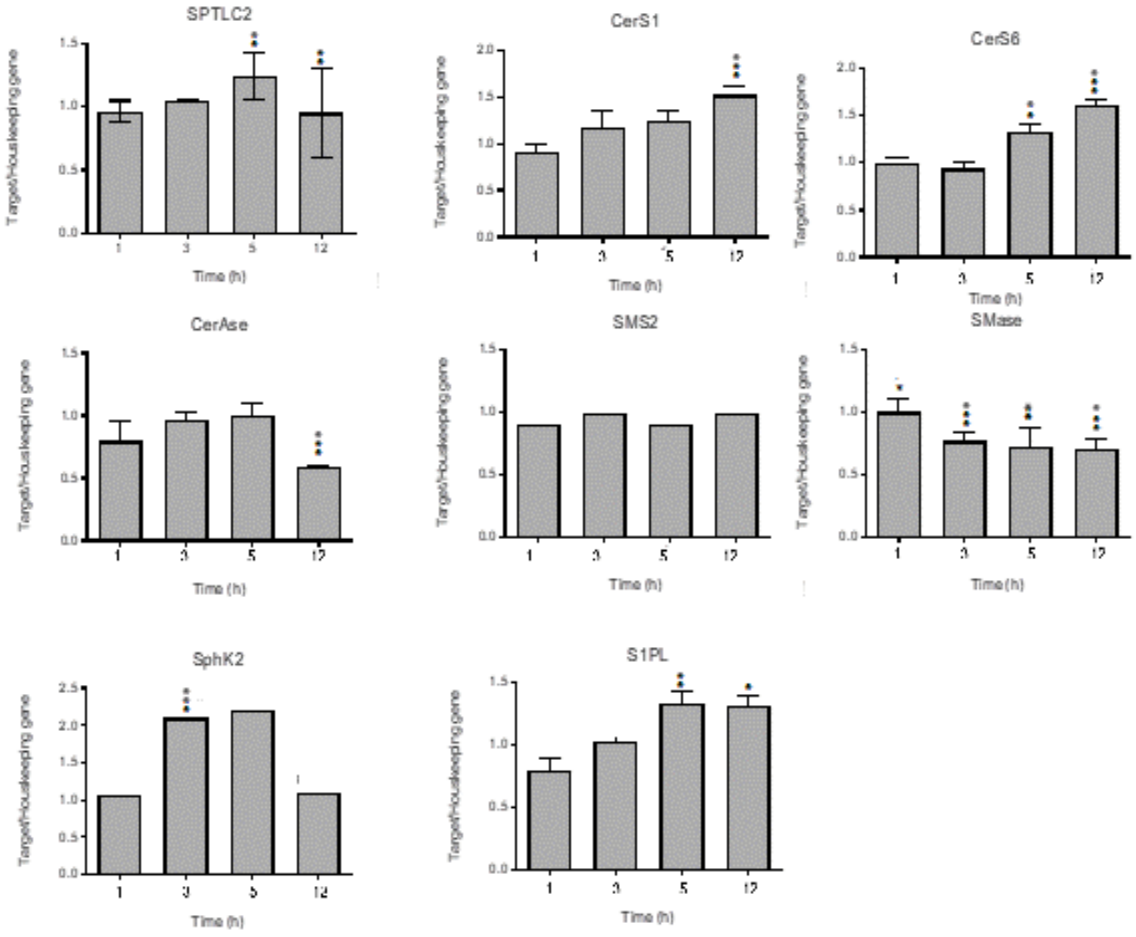

Fig. 8: 2-ClHDA regulates expression of pBMVEC gene products involved in sphingolipid biosynthesis.
pBMVEC were set serum-free overnight and then incubated in the presence of 2-ClHDA (15 µM in DMSO) for the indicated times. Cells were washed, lysed, RNA was isolated and subjected to qPCR analysis. Expression ratios were normalized to HPRT and results were analyzed using the relative expression software tool (REST; *p<0.05, **p<0.01, ***p<0.001; pairwise re-allocation test). At time zero, the ratio of target gene/HPRT expression was set to 1.

4 Discussion

Although the results obtained during my diploma thesis are of a rather preliminary nature, some conclusions can be drawn: In conventional RT-PCR experiments, I could show that self-designed primers directed at the human gene products can be used to reverse transcribe pig RNA into cDNA. This conclusion is substantiated by the fact that several primer combinations yielded the expected amplicon sizes (see **Table 2** and **Fig. 6**). However, it also has to be mentioned that some primer combinations yielded no products. This holds true for the primer combinations directed against the genes ACER1, CerS1, and ASAH1**.** Of interest, primary porcine BMVEC express the RNAs coding for a set of enzymes that are central to a functional SL rheostat including the anabolic and catabolic synthetic pathways as outlined in **Fig. 3** and **Fig**. **4.**

During my qPCR experiments, I have established primer efficiencies, an indispensable measure to assess the performance of a qPCR assay (and equally important, the corresponding dynamic range of the assay). During the experiments performed here, Qiagen primer assays for human genes were used to amplify porcine gene products. This is justified and practicable due to the high homology between human and porcine RNA sequences. Based on a BLAST alignment, orthologous groups were identified in pig/human, and the distribution of sequence similarities of orthologs revealed that the pig is most closely related to cattle with an average amino acid identity of 85.9% while sharing an average identity of 84.1% with humans [57].

In general, qPCR efficiency depends on several factors like operator, instrument type, the number of technical replicates run, quality of serial dilutions, and the chemistry used [56]. The minimal information requirements necessary for publication of qPCR analyses are given in the Minimum Information for Publication of Quantitative Real-Time PCR Experiments (MIQE) publications [58; 59]. Here, I have established PCR efficiency using calibration curves established with dilutions of cDNA samples (**Table 6** and **Fig. 7**). Amplification efficiency (E) was established as outlined by Svec and colleagues [56]. For the establishment of the standard curves, I have plotted the log of template concentration (x-axis) against the C_P values (y-axis) and, by linear regression analysis, determined the slopes of the resulting individual straight lines using GraphPad Prism. Using the slopes,

efficiencies were determined using an open-source calculator from Horizon Discoveries [55]. A theoretical maximum of 1.00 indicates that the amount of product doubles with each cycle [56]. Of note, all my qPCR assays worked with efficiencies slightly lower or higher 100 % (**Table 6**) indicating very good performance. SPTLC2 and SGPL1 were exceptions since E was 115%. Although the reason for this observation is not clear, lower yields at high template concentration might provide a reasonable explanation. This would result in an underestimation of C_P values and too low k-values. According to the equation $E = 10^{-1/slope} - 1$, a slope < 3.332 results in erroneously high values with E>100%.

Taken together, the conventional RT-PCR and RT-qPCR experiments revealed the expression of SPTLC1, SPTLC2 and SPTSSA constituting part of the synthetic complex that is responsible for the first step of SL biosynthesis. SPTLC1 forms a heterodimer with SPTLC2 or SPTLC3 and constitutes the catalytic core. Subunit composition determines substrate specificity: The SPTLC1/2-SPTSSA complex shows preference for C16-CoA whereas the SPTLC1/3-SPTSSA complex uses C14- and C16-CoA as substrate. The pro-inflammatory cytokine TNFA was shown to upregulate SPT activity in endothelial cells (murine lung and human vascular endothelial cells) and this pathway was suggested to be cardioprotective due to increased substrate availability for S1P production [60].

The N-acyltransferases CerS1 and CerS6 that were identified here are highly expressed in mouse brain [61]. CerS1 shows high specificity for C18-Cer synthesis, while CerS6 is specific for C16-Cer synthesis. Both of these enzymes are upregulated in neurodegenerative diseases: In the anterior cingulate cortex of PD patients, a shift in Cer composition towards short acyl-chain length was identified and this lipid composition was accompanied by increased CerS1 expression [62]. In the experimental autoimmune encephalomyelitis model (EAE; a murine model for MS), C16-Cer concentrations were significantly elevated in the lumbar spinal cord and accompanied by increased CerS6 expression in immune cells including astroglia [63].

Cer are degraded by ceramidases and from this gene cluster, I could identify the expression of ACER1/2 and ASAH2. ACER1 is an ER-, while ACER2 is a Golgi-resident alkaline N-acyl hydrolase with both enzymes generating sphingosine and free fatty acids. ACER1 plays an essential role in skin homeostasis, while ACER2 regulates cell proliferation and apoptosis by the production of sphingosine and

sphingosine-1-phosphate and probably ROS [64]. ASAH2 is a neutral plasma membrane ceramidase and together with sphingomyelinases (e.g. SMPD1 or -3 that were also identified during the present work), participates in the production of sphingosine and S1P from the degradation of sphingomyelin, a SL enriched in the plasma membrane of platelets [65].

SMS2 is a transferase that catalyzes phosphatidylcholine transfer to the OH-group of Cer thereby generating SM. In a murine transient middle cerebral artery occlusion stroke model, it was demonstrated that SMS2 deficiency exerted an anti-inflammatory effect in cerebral ischemia-reperfusion through suppression of toll-like receptor 4 recruitment to lipid rafts and inhibition of its downstream signal transduction cascades [66].

SPHK2 identified here has kinase activity and catalyzed the ATP-dependent phosphorylation of sphingosine to S1P. SPHK2 is located on a gene different from SPHK1. In contrast to SPHK1, isoform 2 has a pro-apoptotic function and inhibits cell growth [67]. SPHK1/2 double knockout mice are not viable (double knockouts die at embryonic day 15; knocking out only one isoform does not affect viability) due to defective blood vessel formation, neurogenesis and neural tube closure, indicating that the two isoforms play important roles in embryonic development [68].

SPHK2 also plays an important role in the phosphorylation of Fingolimod (an immune modulating drug that is used for treatment of MS, trade name Gylena). Fingolimod (also called FTY720) acts as pro-drug and after SPHK-mediated phosphorylation (with SPHK2 being 30-fold more active than SPHK1), FTY720-P down-regulates S1P1 receptor expression on lymphocytes and this process leads to significantly lower extravasation of auto-aggressive T-cells across the BBB into the brain [69]. Down-regulation of this receptor reduces astrogliosis, a hallmark of MS, and restores astrocyte-BMVEC communication in MS patients [70] thereby allowing restoration of productive astrocyte communication with other neural cells and BBB. FTY720 and FTY720-phosphate (the active drug that is phosphorylated by SPHK2) were also shown to inhibit drug efflux from the brain by antagonizing P-glycoprotein and leads to increased drug accumulation of e.g. paclitaxel [71], a cytotoxic drug that shows activity in breast cancer patients with brain metastases [72].

2-ClHDA regulates mRNA levels of enzymes involved in the sphingolipid metabolism in pBMVEC. The enzymes, which synthesize ceramides (CerS1 and -6), and S1PL1 were upregulated. It is established that the SL rheostat is affected by inflammatory conditions since TNFα regulates sphingomyelinases, ceramidases, and SPHK1 [21, 73]. In LPS-injected mice Vutukuri [74] could demonstrate that endotoxemia increases serum Cer concentrations (but not in brain or brain capillaries) while S1P concentrations in the serum, whole brain and in brain capillaries of these animals are decreased. In brain capillaries, these observations were ascribed to transcriptional and translational upregulation of S1P phosphatase as well as lipid phosphate phosphatase 1, and to downregulation of SPHK2. In one of our own studies, we observed lower concentrations of Cer and SM species in brain capillaries of LPS-injected mice and these effects could be reverted by the MPO inhibitor ABAH [75].

Taken together, these findings indicate that MPO or MPO-derived oxidants have the potential to interfere with SL homeostasis in vitro and in vivo.

Refe**rences**

1. Sweeney MD, Zhao Z, Montagne A, Nelson AR, Zlokovic BV. Blood-brain barrier: From physiology to disease and back. Physiol Rev. 2019;99(1):21–78.

2. Hawkins BT, Davis TP. The blood-brain barrier/neurovascular unit in health and disease. Pharmacol Rev. 2005;57(2):173–85.

3. Krizanac-Bengez L, Mayberg MR, Janigro D. The cerebral vasculature as a therapeutic target for neurological disorders and the role of shear stress in vascular homeostatis and pathophysiology. Neurol Res. 2004;26(8):846–53.

4. Zlokovic BV. Neurovascular pathways to neurodegeneration in Alzheimer's disease and other disorders. Nat Rev Neurosci 2011;12:723-38.

5. Engelhardt B. Development of the blood-brain barrier. Cell Tissue Res. 2003;314(1):119–29.

6. Ge S, Song L, Pachter JS. Where is the blood-brain barrier ... really? J Neurosci Res. 2005;79(4):421–7.

7. Huber JD, Egleton RD, Davis TP. Molecular physiology and pathophysiology of tight junctions in the blood-brain barrier. Trends Neurosci. 2001;24(12):719–25.

8. Dejana E. Endothelial cell-cell junctions: happy together. Nat Rev Mol Cell Biol. 2004;5(4):261–70.

9. Saitou M, Ando-Akatsuka Y, Itoh M, Furuse M, Inazawa J, Fujimoto K, et al. Mammalian occludin in epithelial cells: its expression and subcellular distribution. Eur J Cell Biol. 1997;73(3):222–31.

10. Saitou M, Furuse M, Sasaki H, Schulzke JD, Fromm M, Takano H, et al. Complex phenotype of mice lacking occludin, a component of tight junction strands. Mol Biol Cell. 2000;11(12):4131–42.

11. Morita K, Sasaki H, Furuse M, Tsukita S. Endothelial claudin: Claudin-5/tmvcf constitutes tight junction strands in endothelial cells. J Cell Biol. 1999;147(1):185–94.

12. Nitta T, Hata M, Gotoh S, Seo Y, Sasaki H, Hashimoto N, et al. Size-selective loosening of the blood-brain barrier in claudin-5-deficient mice. J Cell Biol. 2003;161(3):653–60.

13. Tsukita S, Furuse M, Itoh M. Multifunctional strands in tight junctions. Nat Rev Mol Cell Biol. 2001;2(4):285–93.

14. Muller WA. Leukocyte-endothelial-cell interactions in leukocyte transmigration and the inflammatory response. Trends Immunol. 2003;24(6):327–34.

15. Bazzoni G, Dejana E. Endothelial cell-to-cell junctions: molecular organization and role in vascular homeostasis. Physiol Rev. 2004;84(3):869–901.

16. Lilien J, Balsamo J. The regulation of cadherin-mediated adhesion by tyrosine phosphorylation/dephosphorylation of beta-catenin. Curr Opin Cell Biol. 2005;17(5):459–65.

17. Liebner S, Gerhardt H, Wolburg H. Differential expression of endothelial beta-catenin and plakoglobin during development and maturation of the blood-brain and blood-retina barrier in the chicken. Dev Dyn. 2000;217(1):86–98.

18. Niessen CM. Tight junctions/adherens junctions: basic structure and function. J Invest Dermatol. 2007;127(11):2525–32.

19. Fong CW. Permeability of the blood-brain barrier: Molecular mechanism of transport of drugs and physiologically important compounds. J Membr Biol. 2015;248(4):651–69.

20. Zlokovic BV. The blood-brain barrier in health and chronic neurodegenerative disorders. Neuron. 2008;57(2):178–201.

21. Hannun YA, Obeid LM. Sphingolipids and their metabolism in physiology and disease. Nat Rev Mol Cell Biol. 2018;19(3):175–91.

22. Kuperberg SJ, Wadgaonkar R. Sepsis-associated encephalopathy: The blood-brain barrier and the sphingolipid rheostat. Front Immunol. 2017;8:597.

23. Hannun YA, Obeid LM. Principles of bioactive lipid signalling: lessons from sphingolipids. Nat Rev Mol Cell Biol. 2008;9(2):139–50.

24. Iqbal J, Walsh MT, Hammad SM, Hussain MM. Sphingolipids and lipoproteins in health and metabolic disorders. Trends Endocrinol Metab. 2017;28(7):506–18.

25. Prager B, Spampinato SF, Ransohoff RM. Sphingosine 1-phosphate signaling at the blood-brain barrier. Trends Mol Med. 2015;21(6):354–63.

26. Bienias K, Fiedorowicz A, Sadowska A, Prokopiuk S, Car H. Regulation of sphingomyelin metabolism. Pharmacol Rep. 2016;68(3):570–81.

27. Park W-J, Park J-W. The role of sphingolipids in endoplasmic reticulum stress. FEBS Lett. 2020;594(22):3632–51.

28. Gault CR, Obeid LM, Hannun YA. An overview of sphingolipid metabolism: from synthesis to breakdown. Adv Exp Med Biol. 2010;688:1–23.

29. Patel M. Targeting oxidative stress in central nervous system disorders. Trends Pharmacol Sci. 2016;37(9):768–78.

30. Díaz-Hung ML, González Fraguela ME. Oxidative stress in neurological diseases: Cause or effect? Neurol (Engl Ed). 2014;29(8):451–2.

31. Li Y, Wu P, Bihl JC, Shi H. Underlying Mechanisms and Potential Therapeutic Molecular Targets in Blood-Brain Barrier Disruption after Subarachnoid Hemorrhage. Current Neuropharmacology. 2020;18:1168.

32. Banerjee S, Ghosh S, Mandal A, Ghosh N, Sil PC. ROS-associated immune response and metabolism: a mechanistic approach with implication of various diseases. Arch Toxicol. 2020;94(7):2293–317.

33. Casas AI, Dao VT-V, Daiber A, Maghzal GJ, Di Lisa F, Kaludercic N, et al. Reactive oxygen-related diseases: Therapeutic targets and emerging clinical indications. Antioxid Redox Signal. 2015;23(14):1171–85.

34. Scioli MG, Storti G, D'Amico F, Rodríguez Guzmán R, Centofanti F, Doldo E, et al. Oxidative stress and new pathogenetic mechanisms in endothelial dysfunction: Potential diagnostic biomarkers and therapeutic targets. J Clin Med. 2020;9(6):1995.

35. Khan A, Alsahli M, Rahmani A. Myeloperoxidase as an active disease biomarker: Recent biochemical and pathological perspectives. Med Sci (Basel). 2018;6(2):33.

36. Mano J, Biswas MS, Sugimoto K. Reactive carbonyl species: A missing link in ROS signaling. Plants. 2019;8(10):391.

37. Pizzimenti S, Ciamporcero E, Daga M, Pettazzoni P, Arcaro A, Cetrangolo G, et al. Interaction of aldehydes derived from lipid peroxidation and membrane proteins. Front Physiol. 2013;4:242.

38. Chen C-H, Ferreira JCB, Gross ER, Mochly-Rosen D. Targeting aldehyde dehydrogenase 2: new therapeutic opportunities. Physiol Rev. 2014;94(1):1–34.

39. Nagan N, Zoeller RA. Plasmalogens: biosynthesis and functions. Prog Lipid Res. 2001;40(3):199–229.

40. Skaff O, Pattison DI, Davies MJ. The vinyl ether linkages of plasmalogens are favored targets for myeloperoxidase-derived oxidants: a kinetic study. Biochemistry. 2008;47(31):8237–45.

41. Ford DA. Lipid oxidation by hypochlorous acid: chlorinated lipids in atherosclerosis and myocardial ischemia. Clin Lipidol. 2010;5(6):835–52.

42. Üllen A, Singewald E, Konya V, Fauler G, Reicher H, Nusshold C, et al. Myeloperoxidase-derived oxidants induce blood-brain barrier dysfunction in vitro and in vivo. PLoS One. 2013;8(5):e64034.

43. Wang W-Y, Albert CJ, Ford DA. Alpha-chlorofatty acid accumulates in activated monocytes and causes apoptosis through reactive oxygen species production and endoplasmic reticulum stress. Arterioscler Thromb Vasc Biol. 2014;34(3):526–32.

44. Brahmbhatt VV, Albert CJ, Anbukumar DS, Cunningham BA, Neumann WL, Ford DA. Ω-oxidation of α-chlorinated fatty acids: Identification of α-chlorinated dicarboxylic acids. J Biol Chem. 2010;285(53):41255–69.

45 Ray RS, Katyal A. Myeloperoxidase: Bridging the gap in neurodegeneration. Neurosci Biobehav Rev. 2016;68:611–20.

46. Üllen A, Singewald E, Konya V, Fauler G, Reicher H, Nusshold C, et al. Myeloperoxidase-derived oxidants induce blood-brain barrier dysfunction in vitro and in vivo. PLoS One. 2013;8(5):e64034.

47. Ullen A, Fauler G, Köfeler H, Waltl S, Nusshold C, Bernhart E, et al. Mouse brain plasmalogens are targets for hypochlorous acid-mediated modification in vitro and in vivo. Free Radic Biol Med. 2010;49(11):1655–65.

48. Nusshold C, Üllen A, Kogelnik N, Bernhart E, Reicher H, Plastira I, et al. Assessment of electrophile damage in a human brain endothelial cell line utilizing a clickable alkyne analog of 2-chlorohexadecanal. Free Radic Biol Med. 2016;90:59–74.

49. Üllen A, Fauler G, Bernhart E, Nusshold C, Reicher H, Leis H et al. Phloretin ameliorates 2-chlorohexadecanal-mediated brain microvascular endothelial cell dysfunction in vitro. 2020;1770-1781.

50. Qiagen. RNeasy Plus Mini Handbook [Internet]. Qiagen.com. [cited 3 July 2020]. Available from: https://www.qiagen.com/at/resources/download.aspx?id=16b8f578-d192-4613-ae32-8e02e0b0fa77&lang=en

51 SuperScriptTM III Reverse Transcriptase [Internet]. Fishersci.com. [cited 2020 Jul 3]. Available from: https://assets.fishersci.com/TFS-Assets/LSG/manuals/superscriptIII_man.pdf?_ga=2.21714683.133105730.1609752813-1353441391.1609752813

52 DreamTaq DNA polymerases [Internet]. Thermofisher.com. [cited 2020 Jul 4]. Available from: http://assets.thermofisher.com/TFS-Assets/BID/Reference-Materials/dreamtaq-dna-polymerases-labaid.pdf

53 Quantifast SYBR Green RT-PCR Handbook. Cold Spring Harb Protoc. 2007;2007(11):db.kit25-pdb.kit25.

54 Pfaffl MW, Horgan GW, Dempfle L. Relative expression software tool (REST) for group-wise comparison and statistical analysis of relative expression results in real-time PCR. Nucleic Acids Res. 2002;30(9):e36.

55 qPCR Efficiency Calculator [Internet]. Horizondiscovery.com. [cited 2020 Dec 19]. Available from: https://horizondiscovery.com/en/ordering-and-calculation-tools/qpcr-efficiency-calculator

56 Svec D, Tichopad A, Novosadova V, Pfaffl MW, Kubista M. How good is a PCR efficiency estimate: Recommendations for precise and robust qPCR efficiency assessments. Biomol Detect Quantif. 2015;3:9–16.

57 Fang X, Mou Y, Huang Z, Li Y, Han L, Zhang Y, et al. The sequence and analysis of a Chinese pig genome. Gigascience. 2012;1(1):16.

58 Bustin SA, Wittwer CT. MIQE: A step toward more robust and reproducible quantitative PCR. Clin Chem. 2017;63(9):1537–8.

59 Bustin SA, Benes V, Garson JA, Hellemans J, Huggett J, Kubista M, et al. The MIQE guidelines: minimum information for publication of quantitative real-time PCR experiments. Clin Chem. 2009;55(4):611–22.

60 Zhang Y, Huang Y, Cantalupo A, Azevedo PS, Siragusa M, Bielawski J, et al. Endothelial Nogo-B regulates sphingolipid biosynthesis to promote pathological cardiac hypertrophy during chronic pressure overload. JCI Insight. 2016;1(5).

61 Wegner M-S, Schiffmann S, Parnham MJ, Geisslinger G, Grösch S. The enigma of ceramide synthase regulation in mammalian cells. Prog Lipid Res. 2016;63:93–119.

62 Abbott SK, Li H, Muñoz SS, Knoch B, Batterham M, Murphy KE, et al. Altered ceramide acyl chain length and ceramide synthase gene expression in Parkinson's disease. Mov Disord. 2014;29(4):518–26.

63 Schiffmann S, Ferreiros N, Birod K, Eberle M, Schreiber Y, Pfeilschifter W, et al. Ceramide synthase 6 plays a critical role in the development of experimental autoimmune encephalomyelitis. J Immunol. 2012;188(11):5723–33.

64 Coant N, Sakamoto W, Mao C, Hannun YA. Ceramidases, roles in sphingolipid metabolism and in health and disease. Adv Biol Regul. 2017;63:122–31.

65 Tani M, Sano T, Ito M, Igarashi Y. Mechanisms of sphingosine and sphingosine 1-phosphate generation in human platelets. J Lipid Res. 2005;46(11):2458–67.

66 Xue J, Yu Y, Zhang X, Zhang C, Zhao Y, Liu B, et al. Sphingomyelin synthase 2 inhibition ameliorates cerebral ischemic reperfusion injury through reducing the

recruitment of Toll-like receptor 4 to lipid rafts. J Am Heart Assoc. 2019;8(22):e012885.

67 Orr Gandy KA, Obeid LM. Targeting the sphingosine kinase/sphingosine 1-phosphate pathway in disease: review of sphingosine kinase inhibitors. Biochim Biophys Acta. 2013;1831(1):157–66.

68 Mizugishi K, Yamashita T, Olivera A, Miller GF, Spiegel S, Proia RL. Essential role for sphingosine kinases in neural and vascular development. Mol Cell Biol. 2005;25(24):11113–21.

69 Huwiler A, Zangemeister-Wittke U. The sphingosine 1-phosphate receptor modulator fingolimod as a therapeutic agent: Recent findings and new perspectives. Pharmacol Ther. 2018;185:34–49.

70 Bigaud M, Guerini D, Billich A, Bassilana F, Brinkmann V. Second generation S1P pathway modulators: research strategies and clinical developments. Biochim Biophys Acta. 2014;1841(5):745–58.

71 Cannon RE, Peart JC, Hawkins BT, Campos CR, Miller DS. Targeting blood-brain barrier sphingolipid signaling reduces basal P-glycoprotein activity and improves drug delivery to the brain. Proc Natl Acad Sci U S A. 2012;109(39):15930–5.

72 Kumthekar P, Tang S-C, Brenner AJ, Kesari S, Piccioni DE, Anders C, et al. ANG1005, a brain-penetrating peptide-drug conjugate, shows activity in patients with breast cancer with leptomeningeal carcinomatosis and recurrent brain metastases. Clin Cancer Res. 2020;26(12):2789–99.

73 Clarke CJ, Truong T-G, Hannun YA. Role for neutral sphingomyelinase-2 in tumor necrosis factor alpha-stimulated expression of vascular cell adhesion molecule-1 (VCAM) and intercellular adhesion molecule-1 (ICAM) in lung epithelial cells: p38 MAPK is an upstream regulator of nSMase2: P38 MAPK IS AN UPSTREAM REGULATOR OF nSMase2. J Biol Chem. 2007;282(2):1384–96.

74 Vutukuri R, Brunkhorst R, Kestner R-I, Hansen L, Bouzas NF, Pfeilschifter J, et al. Alteration of sphingolipid metabolism as a putative mechanism underlying LPS-induced BBB disruption. J Neurochem. 2018;144(2):172–85.

75 Goeritzer M, Bernhart E, Plastira I, Reicher H, Leopold C, Eichmann TO, et al. Myeloperoxidase and septic conditions disrupt sphingolipid homeostasis in Murine brain capillaries in vivo and immortalized human brain endothelial cells in vitro. Int J Mol Sci. 2020;21(3):1143.